MIT Open Access Articles

Alumina Nanoparticle Pre-coated Tubing Enhancing Subcooled Flow Boiling Cricital Heat Flux

Proceedings of the ASME 2009 2nd Micro/Nanoscale Heat & Mass Transfer International Conference
MNHMT2009
December 18-21, 2009, Shanghai, China

MNHMT2009-18364

Alumina Nanoparticle Pre-coated Tubing Ehancing Subcooled Flow Boiling Crical Heat Flux

Bao TRUONG[1], Lin-wen HU[2], Jacopo BUONGIORNO[1], and Thomas MCKRELL[1],

[1]MIT Department of Nuclear Science and Engineering, 77 Massachusetts Avenue, Cambridge, MA 02139, U.S.A.
[2]MIT Nuclear Reactor Laboratory, 138 Albany Street, Cambridge, MA 02139, U.S.A.

ABSTRACT

Nanofluids are engineered colloidal dispersions of nano-sized particle in common base fluids. Previous pool boiling studies have shown that nanofluids can improve critical heat flux (CHF) up to 200% for pool boiling and up to 50% for subcooled flow boiling due to the boiling induced nanoparticle deposition on the heated surface. Motivated by the significant CHF enhancement of nanoparticle deposited surface, this study investigated experimentally the subcooled flow boiling heat transfer of pre-coated test sections in water. Using a separate coating loop, stainless steel test sections were treated via flow boiling of alumina nanofluids at constant heat flux and mass flow rate. The pre-coated test sections were then used in another loop to measure subcooled flow boiling heat transfer coefficient and CHF with water. The CHF values for the pre-coated tubing were found on average to be 28% higher than bare tubing at high mass flux G=2500 kg/m^2 s. However, no enhancement was found at lower mass flux G=1500 kg/m^2 s. The heat transfer coefficients did not differ much between experiments when the bare or coated tubes were used. SEM images of the test sections confirm the presence of a nanoparticle coating layer. The nanoparticle deposition is sporadic and no relationship between the coating pattern and the amount of CHF enhancement is observed.

Keywords: Critical Heat Flux, Nanofluid, Boiling-induced Deposition

1. INTRODUCTION

With the constant increase in energy demand, high capacity and efficient power plants will be needed. The power density of them will be higher; therefore, higher heat transfer rate is required to remove heat from the power source efficiently and safely. Nucleate boiling, with its high heat of vaporization, is usually the main heat transfer mechanism to remove heat from such systems. However, nucleate boiling is limited by critical heat flux (CHF), the level at which the heat transfer coefficient drops tremendously due to transition to film boiling. This usually causes damage to the heater. In nuclear reactors with very high power density fuel, reaching CHF is a key safety concern because of possible fuel damage. Therefore, many methods, such using wire wrap, swirl flow, twisted tapes…, have been applied to increase CHF. In light water reactors, a common way to enhance CHF is to use mixing vanes. Recently, nanofluids, colloidal dispersions of nanoparticles in a base fluid [1], have been shown to increase CHF. Even at less than 1.0 vol% particle concentration, up to 200% CHF compared to that of the base fluids were measured for pool boiling (You et al. [2] and Kim et al. [3]). Other researchers, such as Vassallo et al [4], Tu et al. [5], Kim and Kim [6], Moreno et al. [7], Bang and

Chang [8], Milanova et al. [9], Jackson et al. [10] and Wen and Ding [11], measured CHF enhancements of varying magnitudes. For flow boiling, very few studies of nanofluids have been reported in the literature. In our laboratory, subcooled flow boiling CHF of different nanofluids at different mass fluxes were measured at atmospheric pressure. The results show CHF enhancement up to 50% while the heat transfer coefficients of nanofluids are within 20% of that of water. These were reported in reference [12] and [13].

It should be noted that in nanofluids, materials used for nanoparticles include chemically stable metals (e.g., gold, silver, copper), metal oxides (e.g., alumina, zirconia, silica, titania) and carbon in various forms (e.g., diamond, graphite, carbon nanotubes). Base fluids commonly used for nanofluids include water, refrigerants, ethanol, and ethylene glycol. Nanoparticles can remain dispersed without significant pH and agglomeration by controlling their surface properties through use of surfactants. It is also expected that nanofluids can remain stable over a long period of time with little erosion and gravitational settlement.

One common finding in the CHF studies was that the nanoparticle deposited on the heater's surface during the boiling process in both pool and flow boiling experiments. For example, nanoparticle depositions on heater surfaces were reported by Bang and Chang [8], and Kim et al. [14]. Liu and Qui [15] reported a thin sorption layer on the heated surface when a nanofluid jet impinges on the surface. The depositions of nanoparticles were found to change the heater surface morphology. Since the thermophysical properties (surface tension, thermal conductivity, viscosity, evaporation heat, specific heat, density) of dilute nanofluids are similar to that of pure water, the changes in surface morphology are believed to be among the mechanisms for the CHF enhancement of nanofluids. For example, Kim et al. [16] reported a CHF enhancement due to nanoparticle deposition on the heated surface of a wire. In their experiment, TiO_2 nanoparticle coated NiCr wires were prepared through boiling nanofluids of various concentrations. The coated wires were subsequently tested in water and up to 200% CHF enhancement was obtained.

While surface modification to enhance CHF and heat transfer coefficient is well known, the use of boiling-driven nanoparticle deposition for such application is a novel concept since nanofluid research has captured wide interests only in the last decade. In our laboratory [17,18] preliminary experiments of boiling-driven deposition have been done on SS-316 and nickel wires in alumina nanofluids. After 15 to 60 minutes o

boiling time at 0.5 MW/m^2, the deposition thickness on a stainless steel wire varied from 1.5 to 3 micrometers for alumina deposited layer on the wire. The alumina coating layer was a lot more consistent compared to that of diamond. This proof of concept of boiling enhanced deposition in nanofluid was then applied to the test sections of a flow loop.

The objective of this study is to measure the flow boiling heater transfer coefficient and CHF of heat transfer surfaces pre-coated with nanoparticles. In the experiments reported here, stainless steel test sections were pre-coated with nanoparticles via boiling-induced deposition of dilute alumina nanofluids. These pre-coated test sections were then used to perform flow boiling experiments in pure water. Heat transfer coefficient and CHF of the pre-treated and untreated test sections are compared to evaluate the performance of the nanoparticles pre-treated test sections.

2. EXPERIMENTS

2.1. Nanofluid Preparation and Characterization

The alumina nanofluid used in the experiments was purchased from Nyacol. The as-purchased concentration was 20% by weight, or 6 vol%. The as-received concentration was verified in our lab using neutron activation analysis and thermo-gravimetric analyzer. The mean diameter of the alumina nanoparticle was measured using dynamic light scattering analyzer and found to be about 40nm, as specified by the vendor. The alumina nanofluid was stabilized using nitric acid and no surfactant was used. The alumina nanofluid used in pre-coating the test sections ranged from 0.1% to 1.0 vol% and was prepared through dilution using deionized water only. Tests were conducted previously in our lab [19] which confirmed that the diluted alumina nanofluid maintained its stability and particle size.

2.2. Pre-coating of Test Section via Flow Boiling

The test sections were pre-coated using a separate loop, known as coating loop, whose schematic is shown in Figure 1. The coating loop is constructed of stainless steel tubing of 0.25" (6.35mm) OD and consists of a test section assembly of the same dimension of that used in the flow boiling loop (described below), a pump and an accumulator/heat exchanger system. The procedure to coat a test section is as follows. First, approximately 3500 ml of nanofluid was added to the accumulator. The fluid was then circulated around the loop using the centrifugal pump. The flow rate was controlled using a needle valve in the bypass loop.

Once the flow rate (G = 670 kg/m^2s), was established, a desired heat flux was applied to the test section via the copper electrodes using a DC power supply. The bulk fluid temperature was monitored and controlled (by adjusting chilled water flow rate) so that the inlet temperature stayed relatively constant once it reached equilibrium. The coating process lasted 1-2 hours after equilibrium was established to allow particle deposition. Table 1 lists the different coating conditions. There are four sets of pre-coated test sections. For each set of test sections, a new reservoir of nanofluid was used, even if coating conditions between each set were identical.
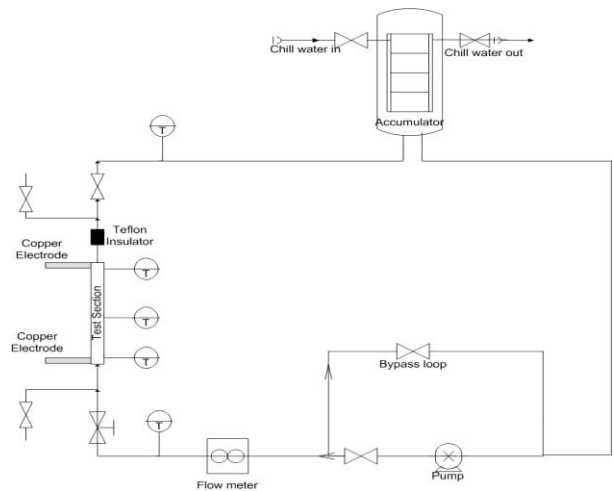

Fig. 1: Schematic diagram of coating loop

Table 1: Summary of Coating conditions

Test section	Coating Fluid	Coating Heat flux	Coating Time
C1	0.1 vol% Alumina	1.0 MW/m^2	1.5 hours
C2			
C3			
C4			
C5	1.0 vol% Alumina	1.0 MW/m^2	2 hours
C6			
C7			
C7*			
C8	1.0 vol% Alumina	1.5 MW/m^2	2 hours
C9			
C10			
C11			
C12	1.0 vol% Alumina	1.5 MW/m^2	2 hours
C13			
C14			

2.3. Flow Boiling CHF Experiment

The CHF experiments were conducted in the flow boiling loop as shown in Figure 2. The working fluid is deionized water. This loop contains a test section, a pre-heater, a heat exchanger, a pump and an accumulator. The loop was constructed mostly with 25.4 mm OD (1") stainless steel tubing. The stainless steel 316 test section (purchased from All Stainless Inc., Ship # 302850, ASME SA213-014 HEAT No 1471/0654 BA) has OD of 6.35 mm (0.25") with wall thickness of 0.41mm (0.016"). The heated length is 100 mm. The detail of the test section is shown in Figure 3.

Power is supplied to the test section via the end's copper electrodes, which are connected to two identical DC power supplies operating in parallel. The voltage and the current supplied to the test section are measured using calibrated voltmeter and inductive ammeter with uncertainty less than 2%. The heat flux on the inner tube surface is calculated as:
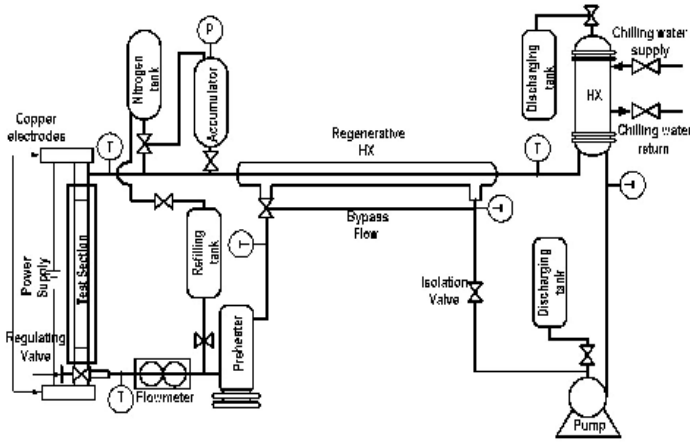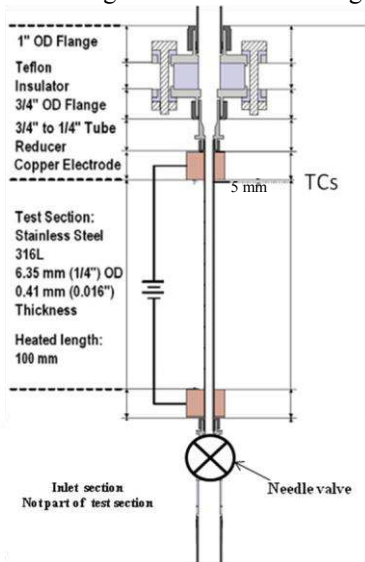
2

Fig. 2: Schematic diagram of the flow boiling loop

Fig. 3: The schematic of the test section

$$q" = \frac{IV}{\pi D_i L} \qquad (1)$$

where V and I are the voltage and current, respectively, and D_i and L are the inner diameter and the heated length of the test section, respectively. The uncertainty in the measurement of the heat flux is $<\pm4\%$. K-type thermocouples are used to measure the inlet and outlet temperature of the test section. Several K-type thermocouples are clamped onto the outer surface of the tubing at different azimuthally locations right below the top copper electrodes to measure the outer wall temperatures. The heat loss (defined as the normalized difference between the electric power and the fluid thermal power) are estimated to be less than 10% at low heat flux ($q"<$ 1.0 MW/m^2) and less than 5% at high heat flux ($q"<$ 4.5 MW/m^2). The pressure can be controlled using the accumulator but all experiments were performed at atmospheric pressure. The accumulator is also used to purge non-condensable gas at the beginning of each run. The centrifugal pump was used to control mass flow rate in the loop, which was measured with a flow meter of $<\pm5\%$ uncertainty.

The flow boiling experiment procedure using untreated, bare tubing is as follows. The test section was first cleaned with acetone to remove possible contaminant. After filling up the loop with water, degassing was performed at 60ºC for approximately one hour. Further degassing was done through boiling by applying approximately 2.8 – 3.0 MW/m^2 heat flux

to the tube for 30 minutes. The temperature of the fluid was kept at 60ºC throughout this process. After degassing, the power was turned off and fluid temperature was reduced to the inlet chill water temperature. The mass flux was established and then power was supplied to the tube in constant steps. Three-minute wait allowed steady state to be achieved between each step. Flow rate, test-section current and voltage, inlet and outlet temperature and wall temperature were recorded and monitored at each step simultaneously. The power increase continued until CHF occurred, usually indicated by rupture of the test section.

The procedure to measure CHF using a pre-coated test section was similar to that when a bare tube was used except during the degassing phase. A bare tube was used in the first hour of degassing at 60ºC. This bare test section was then replaced with the pre-coated test section. The procedure used for pre-coated test section experiment was identical to that of untreated tube.

3. RESULTS

3.1. Critical Heat Flux

The CHF values of water measured using bare tubes and pre-coated tubes are listed in the Table 2. Bare means untreated tubes. "NA" in the table indicates that CHF test was not measured using that test section. The uncertainty in the measured heat flux is $<\pm4\%$. The CHF values of untreated test sections agreed well with the 1995 lookup table (LUT) values [20], which verified that the flow loop performed as expected.

Table 2: Summary of CHF value of water

Fluid	G kg/m^{2}s	Measured CHF MW/m^2	Xe	LUT CHF	Meas. / LUT CHF
Bare-1	2500	5.40	-0.072	5.34	1.01
Bare-2	2500	5.51	-0.072	5.35	1.03
Bare-3	2500	5.32	-0.079	5.58	0.95
C1	2500	6.20	-0.063	5.23	1.19
C2	2500	6.48	-0.059	5.19	1.25
C3	2500	6.51	-0.058	5.17	1.26
C4	NA	NA	NA	NA	NA
C5	2500	7.15	-0.043	4.93	1.45
C6	2500	6.14	-0.059	5.19	1.18
C7	2500	6.27	-0.059	5.19	1.21
C7*	NA	NA	NA	NA	NA
C8	2500	6.88	-0.051	5.09	1.35
C9	2500	7.10	-0.053	5.11	1.39
C10	2500	6.88	-0.056	5.15	1.34
C11	NA	NA	NA	NA	NA
C12	1500	5.01	-0.043	4.96	1.01
C13	1500	5.11	-0.042	4.95	1.03
C14	NA	NA	NA	NA	NA

Test sections C1-C4 enhanced CHF by 23% on average, while C5-C7 had 28% CHF enhancement. C8-C11 gave highest CHF enhancement (35% on average). Notice that the CHF enhancement is higher for test sections coated at higher heat flux and longer time. This could mean that high heat flux and

3

Copyright © 2009 by ASME

longer time allow more coating of nanoparticles on the test section. SEM images (shown in a later section) can help to verify this. While the CHF enhancement for these three batches is somewhat lower than that reported by Kim et al. [12, 13], they are consistent within each batch (within 10%), except for that of C5. Nevertheless, these results provide encouraging confirmation that boiling-induced deposition is one possible way to deposit nanoparticles on heated surfaces, to enhance CHF effectively.

Notice that C12-C14 test sections were used to measure CHF of water at mass flux of only 1500 kg/m²s and no enhancement was observed. This is consistent with what was observed by Kim et al.[13], who previously measured no CHF enhancement of nanofluids (Alumina, Zinc Oxide and diamond) at the same mass flux using the exact two phase loop presented here. As of now, we are still investigating possible models to explain why CHF enhancement at high mass flux of 2500 kg/m²s but not at low mass flux of 1500 kg/m²s.

3.2. Heat Transfer Coefficient

The heat transfer coefficient (HTC) was calculated from the wall temperatures measured using the K-type TCs distributed axially. The inner wall temperature, T_{wi}, was calculated using the radial heat conduction equation in the tube wall with appropriate boundary conditions.

$$T_{wi} = T_{w,out} - q'' \frac{D_i}{2k_h} \left[\frac{D_o^2}{D_i^2 - D_o^2} \ln \frac{D_i}{D_o} - \frac{1}{2} \right] \quad (2)$$

D_o and D_i are the outer and inner diameter, respectively. $T_{w,out}$ is the outer wall temperature (measured by TCs). k_h is the thermal conductivity of stainless steel test section, whose temperature dependence is given as:

$$k_h = 13.00857 + 0.01687 T_w \\ - 2.08333 \times 10^{-6} T_w^2 \quad (3)$$

which represents a best fit of the SS316 thermal conductivity values reported in the ASME code [21]. T_w here is the average wall temperature.

The effective heat transfer coefficient, h, then can be calculated using the measured heat flux, the bulk temperature and the inner wall temperature as:

$$h = \frac{q''}{T_{w,i} - T_b} \quad (4)$$

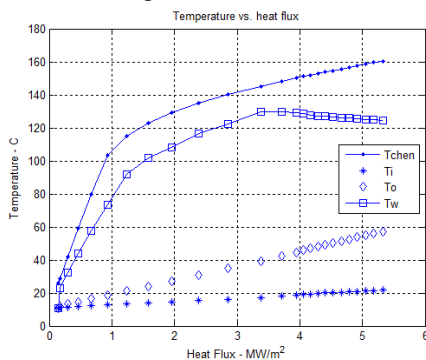where T_b is the bulk temperature at the outlet of the test section.

Fig. 4: Representative temperature vs. heat flux

Figure 4 shows representative temperature profile as a function of heat flux. Here, the T_{chen} is the wall temperature calculated

with the well known Chen correlation, using the measured heat flux and the outlet bulk temperature as inputs.

Figure 5 shows the heat transfer coefficient measured for bare test sections. The values between three bare test sections within measurement uncertainty, which is 10% at most. The values predicted by the Chen correlation are lower than the measured ones. The results here agree with what were measured previously in our laboratory by Kim et al. [12].
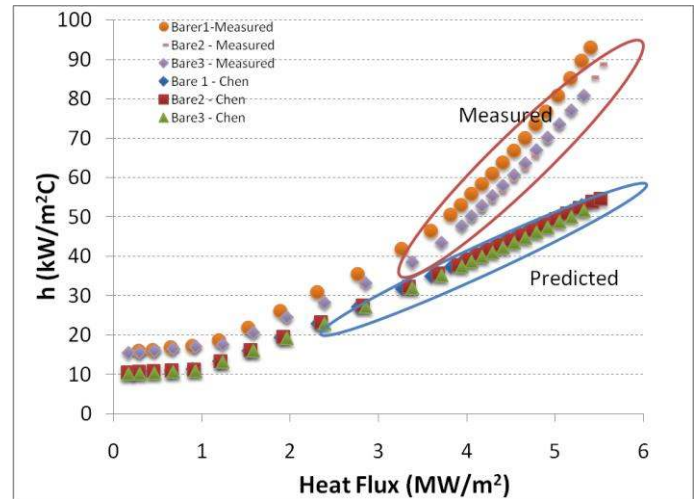

Fig. 5: Comparison of measured and predicted heat transfer coefficient for bare test section (uncertainty of 10%)

Figure 6 compares the heat transfer coefficient measured with different coated test sections compared to that of the bare tube. To simplify the graphs, the predicted values using Chen correlation (which are also lower than the measured ones) are not shown in this figure. There appears to be no change in heat transfer coefficient at all between the coated test sections and the bare ones. However, this can be only observed up to CHF measured with the bare tube. Beyond this heat flux, no comparison can be made because no HTC value could be measured for the bare tube. Nevertheless, it should be expected by extrapolation that no abnormal change in heat transfer coefficient would be seen at higher heat flux. The heat transfer coefficient for C8, C9, C10, C16 and C17 followed the same trend of that of bare test sections, as shown in Figure 7.
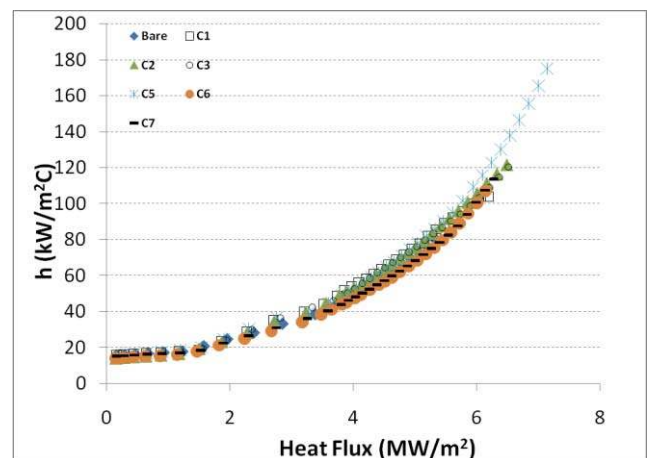

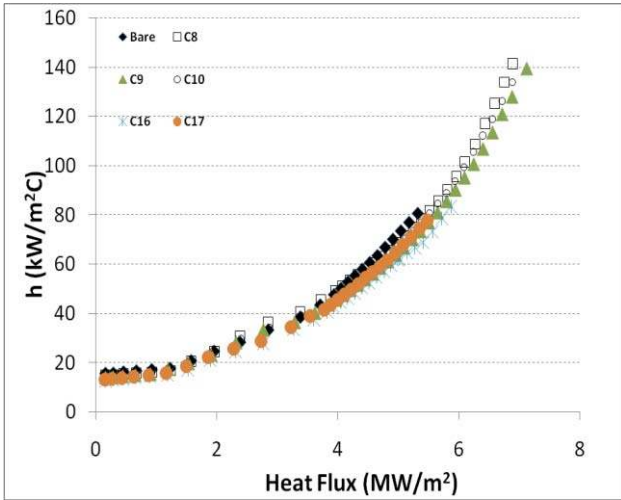Fig. 6: Measured heat transfer coefficient of C1 to C7 test section (uncertainty of 10%)

4

Copyright © 2009 by ASME

Fig. 7: Measured heat transfer coefficient of C8-C10 and C16-C17 test sections (uncertainty of 10%)

3.3. Surface Characterization

After CHF experiment, the test section was cut using Electrical Discharge Machine (EDM) into four quarters of length approximately 1.25 cm from the burn-out location. Scanning Electron Microscopy (SEM) and Energy Dispersive Spectroscopy (EDS) of the cut test sections were then examined. The results are shown in Figure 8 and Figure 9. In Figure 8, representative pre-coated test sections from different batches show some Alumina particle deposited on the surfaces. However, none of them shows a uniform coating layer. The stainless steel substrate could be observed here. In Figure 9, higher magnification SEM images of test sections of various batch is shown with their associate EDS. For the bare-1 test section, only Iron and Chromium peaks are observed as they are main elements in stainless steel. Spherical Alumina particles could be observed clearly on test sections C1, C5, C10 and C13. In addition, Alumina and Oxygen are the dominant peaks seen in the EDS spectrum. This means the deposited layers are indeed made of alumina and they must be several-micron thick to prevent stainless steel to be detected by EDS.

4. CONCLUSIONS

Subcooled flow boiling CHF enhancement up to 28% on average was measured using test sections pre-coated with alumina nanoparticles. The pre-coating was performed via flow boiling alumina nanofluid. However, CHF enhancement was only observed at high mass flux G=2500 kg/m^2 s and no enhancement was found at lower mass flux G=1500 kg/m^2 s. More investigation of models to explain the difference between the two mass fluxes need to be done. SEM images confirmed the presence of nanoparticle on the pre-coated surface. However, the coating is not uniform. The heat transfer coefficients were found to be the same for the bare and the coated test sections within measurement uncertainty, and both are higher than the predicted values using the Chen correlation.
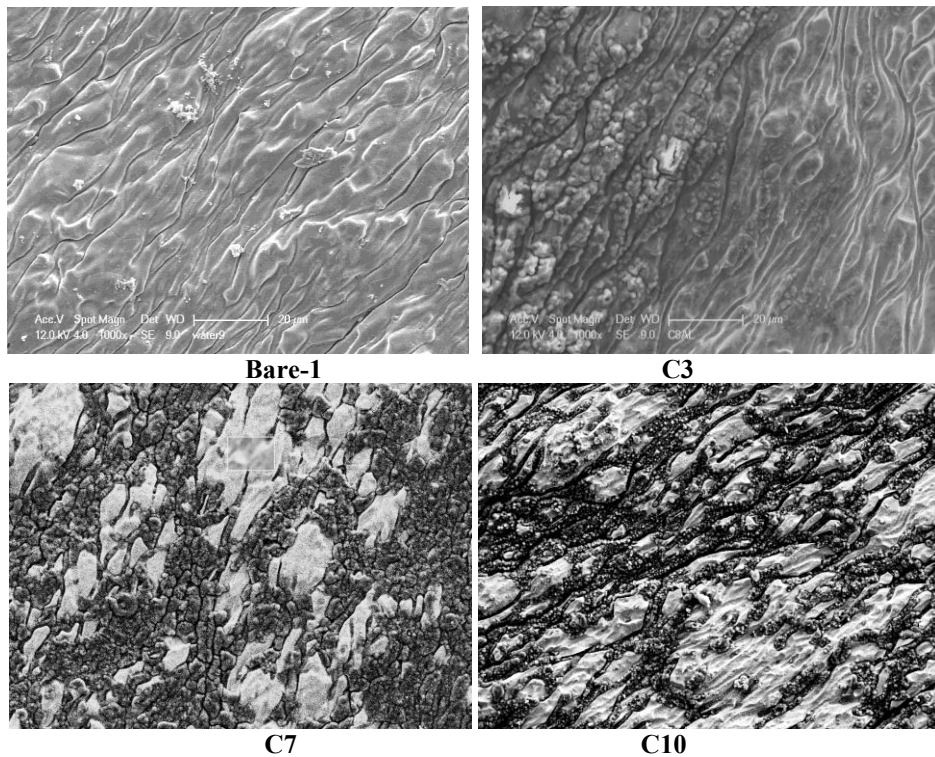
Bare-1

C3

C7

C10

Fig. 8: Representative SEM images (approximately 1000X magnification) of test sections that ran in two-phase loop.
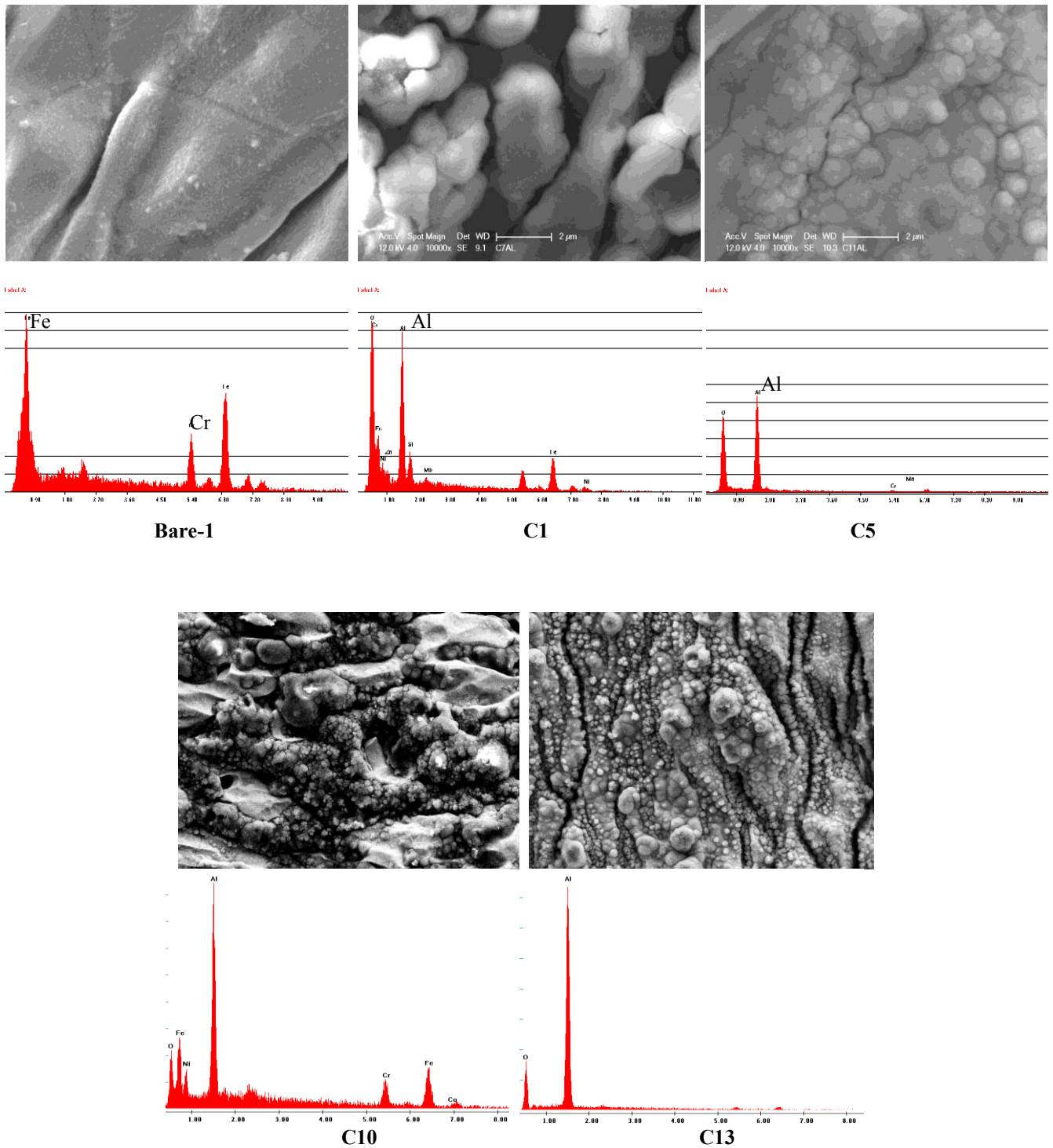
5

Copyright © 2009 by ASME

Fig. 9: Representative SEM images at higher magnification (approximately 10000X) and their associate EDS spectrum

REFERENCES:

1. S. U. S. Choi, "Enhancing Thermal Conductivity of Fluids with Nanoparticles", In: D. A. Siginer, &H. P. Wang. Eds. Developments and Applications of Non-Newtonian Flows,. ISBN: 0791817423. ASME FED-231/MD-66 pp.99-205, 1995.

2. S. M. You, J. Kim, and K. H. Kim, Effect of nanoparticles on critical heat flux of water in pool boiling heat transfer, *Applied Physics Letters* 83 (16) (2003) 3374-3376.

3. H. Kim, J. Kim, and M. Kim, Experimental study on CHF characteristics of water-TiO2 nano-fluids, *Nuclear Engineering and Technology* 38 (1) (2006).

4. P. Vassallo, R. Kumar, and S. D'Amico, Pool boiling heat transfer experiments in silica-water nano-fluids, *Int. J. of Heat and Mass Transfer* 47 (2004) 407-411.

5. Tu J. P., N. Dinh, T. Theofanous, An experimental study of nanofluid boiling heat transfer, Proceedings *of 6th International Symposium on Heat Transfer*, Beijing, China. 2004.

6. H. D. Kim and M. H. Kim, Critical heat flux behavior in pool boiling of water-TiO2 nano-fluids, *Proceedings of Fourth Japan-Korea Symposium on Nuclear Thermal Hydraulics and Safety*, Sapporo, Japan, Nov. 28-Dec 1, 2004.

7. G. Moreno Jr., S. Oldenburg, S. M. You, and J. H. Kim, Pool Boiling Heat Transfer of Alumina-Water, Zinc Oxide-Water and Alumina-Water Ethylene Glycol Nanofluids, *Proceedings of HT2005*, San Francisco, California, USA, July 17-22, 2005.

8. I. C. Bang and S. H. Chang, Boiling Heat Transfer Performance and Phenomena of Al2O3-Water Nano-fluids from a Plain Surface in a Pool, *Int. J. of Heat and Mass Transfer,* 48 (2005) 2407-2419.

9. D. Milanova, R. Kumar, S. Kuchibhatla, S. Seal, Heat transfer behavior of oxide nanoparticles in pool boiling experiment, *Proc. of 4th International Conference on Nanochannels, Microchannels and Minichannels, Limerick, Ireland*, June 19-21, 2006.

10. J. E. Jackson, B. V. Borgmeyer, C. A. Wilson, P. Cheng, and J. E. Bryan, Characteristics of nucleate boiling with gold nanoparticles in water, *Proceedings of IMECE 2006, Chicago, 2006.*

11. D. Wen and Y. Ding, Experimental Investigation into the Pool Boiling Heat Transfer of Aqueous Based γ-alumina nanofluids, *Journal of Nanoparticle Research* 7 (2005) 265-284.

12. S. J. Kim, T. McKrell, J Buongiorno, and L.W. Hu, "Subcooled Flow Boiling Heat Transfer of Dilute Alumina, Zinc Oxide , and Diamond Nanofluids at Atmospheric Pressure", *NUTHOS-7*: *International Topical Meeting on Nuclear Reactor Thermal Hydraulic, Operation and Safety*, Seoul, Korea, October 5-9, 2008.

13. S. J. Kim, T. McKrell, J Buongiorno, and L.W. Hu, "Experimental Study of Flow Critical Heat Flux In Alumina-Water, Zinc-oxide-Water and Diamond-Water Nanofluids", *J. Heat Transfer*, 131(4), 2009..

14. S. J. Kim, I. C. Bang, J. Buongiorno, and L. W. Hu, Surface Wettability Change during Pool Boiling of Nanofluids and its effect on Critical Heat Flux, *Int. J. Heat Mass Transfer* 50 (19-20) (2007) 4105-4116.

15. Z.-H. Liu and Y.-H. Qui, Boiling Heat Transfer Characteristics of Nanofluids Jet Impingement on a Plate Surface*, J. Heat Mass Transfer,* 43 (2007) 699-706.

16. H. Kim and M. Kim, Experimental Study of the Characteristics and Mechanism of Pool Boiling CHF Enhancement Using Nanofluids, *J. Heat Mass Transfer, Special Issue*, (2007).

17. B. Edwards, "Effect of Combined Nanoparticle and Polymeric Dispersions on Critical Heat Flux, Nucleate Boiling Heat Transfer Coefficient, and Coating Adhesion" M.S. Thesis, MIT, June 2009

18. B. Truong, "Determination of Pool Boiling Critical Heat Flux Enhancement in Nanofluids", B.S. Thesis, MIT, June 2007

19. J. Buongiorno, L.-W. Hu, S. J. Kim, R. Hannink, B. Truong and E. Forrest, "Nanofluids for Enhanced Economics and Safety of Nuclear Reactors: An Evaluation of the Potential Features, Issues and Research Gap", *Nuclear Technology,* 162(1), 80-91, 2008.

20. D. C. Groeneveld, J. Q. L.K.H. Leung, P. L. Kirillov, V.P. Bobkov, I. P. Smogalev, V.N. Vinogradov, X.C. Huang and E. Royer, "The 1995 CHF Look-up Table for Critical Heat Flux in Tube", *Nuclear Engineering and Design*, 163, 1-23, 1996.

21. American Society of Mechanical Engineers (ASME). *Boiler and Pressure Vessel Code*. Case N-47-30, Section III, Division I. 1992

7

Copyright © 2009 by ASME